ORIGINAL ARTICLE

Experimental and simulated study of 3D-printed couplings' suitability for industrial application

Nuria Baladés[1] · Paula Remigio[2] · David L. Sales[3] · Daniel Moreno[4] · Jesús M. López[5] · Sergio I. Molina[6]

Abstract

This paper explores the possibility of applying reverse engineering to flexible coupling spare parts through additive manufacturing. Although couplings' simplicity makes them go unnoticed, they connect elements that transmit power between two shafts, thus being an essential component for most of the machinery currently used in the industry. In this study, flexible couplings with different infill density (60% and 80%) were 3D printed by the fused filament fabrication technique. The original and the additive manufactured couplings were modelled to compare their compressive response and energy-absorbing characteristics, and experimental tests were performed to validate finite element analysis. To derive an optimal material distribution within coupling structure, a generative design approach was conducted through nTopology software. With this novel simulation-driven design, it is possible to reduce the weight of the redesigned part up to 15.8% by defining the wall thickness of the internal structure based on the results of finite element simulation, while maintaining its functionality. Moreover, an economic-environmental study was carried out. Results ensure that the 3D printed prototypes are suitable for replacing the original one under its current operating conditions. Additionally, the economic study shows that the redesigned couplings allow companies to save more than €2700 per coupling in relation to CO_2 emission payments.

Keywords Reverse engineering · 3D printing · Industry 4.0 · Additive manufacturing · Spare parts · Simulation · Field-driven design

✉ Nuria Baladés
nuria.balades@uca.es

1 IEG Group, Department of Industrial Engineering and Civil Engineering, IMEYMAT, Algeciras School of Engineering and Technology, Universidad de Cádiz, Algeciras, Cádiz, Spain

2 PAIDI-TIC-168 Group, Department of Automation Engineering, Electronics, Architecture and Computer Networks, Algeciras School of Engineering and Technology, Universidad de Cádiz, Algeciras, Cádiz, Spain

3 INNANOMAT Group, Department of Materials Science Metallurgical Engineering and Inorganic Chemistry, IMEYMAT, Higher Technical School of Engineering, Universidad de Cádiz, 11202 Algeciras, Cádiz, Spain

4 INNANOMAT Group, Department of Mechanical Engineering and Industrial Design, Higher Technical School of Engineering, Universidad de Cádiz, Puerto Real, Spain

5 Maintenance Department, INDORAMA Ventures Química SLU, San Roque, Spain

6 INNANOMAT Group, Department of Materials Science Metallurgical Engineering and Inorganic Chemistry, IMEYMAT, Facultad de Ciencias, Universidad de Cádiz, Campus Río San Pedro, 11510 Puerto Real, Cádiz, Spain

1 Introduction

The fourth industrial revolution or Industry 4.0 is increasingly being implemented in several industries. This paradigm shift related to information management, together with the application of novel technologies to production ecosystems, has gone beyond both the most sophisticated industries (e.g., aeronautics and automobile industries) and all kinds of production environments (e.g., chemical industry, mass production goods, food and maritime industry). Enabling technologies are being widely used, so factories are evolving towards the concept of factories of the future (FoF), thus changing production and management processes [1]. These technologies are based on connectivity and intercommunication. Big data, simulation, internet of things, novel materials, virtual reality, reverse engineering, robotics and additive manufacturing are the key enabling technologies [2]. Likewise, several production technologies have also contributed.

One of the most reliable applications of these technologies in production plants is the combined use of reverse engineering and additive manufacturing (AM) to replicate spare parts damaged while being used. This combination

Table 1 Maximum in-service values given by the manufacturers of the original coupling [23]

Parameter	Maximum in-service values
Nominal torque	200 N·m
Maximum torque	500 N·m
Maximum speed	4.500 rpm
Torsional stiffness	4.200 N·m/rad

reduces time and cost when spare parts are produced in-house instead of by the original manufacturer [3–5]. This approach has been widely studied. Liu and Ghadge were among the first to publish research on the positive impact of AM on aircraft spare parts [6]. Moreover, the benefits and drawback of the implementation and production of spare parts in the maritime industry have been recently defined [7]. The automotive industry has implemented this production model to analyse the impact of the remote production of spare parts in developing countries [8]. This approach is also used by the European automotive industry from a more strategic point of view when selecting industrial stakeholders. As a result, adopting AM positively impacts supply chain flexibility and performance [9].

Reverse engineering was widely used during World War II, when enemy armies seized war supplies such as aircraft or other war machinery to improve their own machinery though an exhaustive analysis. Today, it is used in various fields, specially in medical, aerospace and industrial sectors [10–12].The process involves working backward through the original design process, thus obtaining a new geometry from a manufactured element and digitalizing and editing a computer-aided design (CAD) 3D model. This method has greater risk than the traditional engineering processes based on a first design lately manufactured by one or several technologies and assembled [13]. However, reverse engineering process allows engineers to work without technical data, e.g., material properties or technical drawings. Furthermore, this process could be used to reduce both downtimes and materials stocks in machine maintenance, thus optimising enterprise economic resources.

Due to the great advances in AM, reverse engineering can be used for industrial purposes, including prototype creation and decentralized production of components (i.e., final pieces) [14], and it is among the most remarkable technological bases of the rising Industry 4.0 [2]. This technique, also known as 3D printing technique, uses a CAD software to control the deposition material layer-by-layer in precise and complex geometric shapes. There are many AM methods, so choosing the appropriate technique is something of a challenge. Various methods and compatible materials should therefore be analysed before the design stage [15, 16]. Furthermore, environmental factors can significantly influence both the price of manufactured components and their use cost during their lifetime. The tax for both CO_2 emissions and carbon footprints is increasing every year. According to the European CO_2 Trading System, the average tax for CO_2 emissions has reached €83.03 per CO_2 emitted ton in 2022, i.e., eleven times higher than 10 years ago [17].

Moreover, AM techniques due to their limitless complexity in manufacturing are ideal candidates to be combined with generative design such as topological optimization. Topological optimization is a numerical method that refines the placement of material within a user-defined design space. By providing the software with boundary conditions and constraints, objectives such as maximizing the stiffness or reducing the weight of a component can be achieved [18, 19]. Along these lines, the field-driven design allows the creation of elements that would be very difficult to obtain by any other means. Through the use of scalar or vector fields, a convenient way to manage complex geometries is offered, together with a capability that allows users full control over variations in size and shape from one point in space to another, providing unprecedented design freedom and flexibility [20, 21].
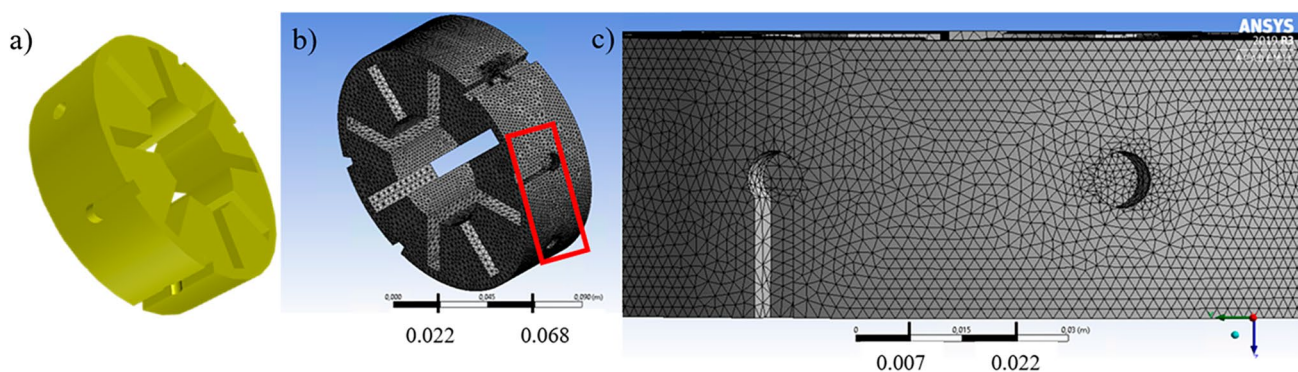

Fig. 1 **a** Coupling 3D CAD design. **b** Established mesh for the couplings. **c** Meshing details represented with a red square in **b**

Table 2 Safety factor parameters [23]. Selected values for the study case are highlighted in bold in the table

Machine	Electric engines	4 to 6 cylinders petrol engines		1 to 3 cylinders petrol engines	
F1: Type of motor in the machine					
With medium masses to accelerate and irregular operation	1.8	2.0		**2.8**	
F2: Operation period (hours/day)					
More than		2		12	
Until	2	12		24	
F2 factor	1	1.15		**1.3**	
F3: Starts per hour					
More than		10	40	120	200
Until	10	40	120	200	
F3 factor	1	**1.25**	1.75	2.5	3

This work aims to apply reverse engineering and a suitable 3D printing technique to redesign and build a common spare part in industry. Specifically, the component consists of a flexible coupling that links the input and output transmission shafts between an electric motor and a booster pump. Both the materials for AM and the AM method were selected according to the specifications—thermoplastic polyurethane (TPU) and fused filament fabrication (FFF), respectively [16, 22]. Moreover, two density models were 3D printed, and their properties and functionality were compared to the original coupling. Additionally, an eco-audit was performed using the ANSYS Granta Edupack software to estimate the energy consumption and carbon footprint of the couplings' life cycle. Finally, a simulation field-driven design derived from the scalar stress field generated by FEA was conducted to optimise the redesign coupling's weight, using the nTopology software.

2 Materials and methods

In our study, we use reverse engineering to obtain a cheaper industrial-compatible product using a different manufacturing process, so we start from a polyurethane elastomer (TPU) coupling manufactured by reaction-injection moulding (RIM) and, based on its dimensions and properties, we study the feasibility of manufacturing it by an AM technique.

2.1 Process and material selection

The first step to redesigning an industrial element consists of selecting the optimum procedure among the existing ones. For this purpose, the database of GRANTA Edupack software was used. This software provides access to a comprehensive database of more than 3900 materials and processes. It also permits browsing for material properties, as well as material and process selection by considering the requirements of the final part. The procedure followed for the selection of the additive manufacturing process is (i) collection of the available additive manufacturing methods, (ii) screening the candidates using both process and materials characteristics which work properly with each other, (iii) re-ordaining those printing methods which meet the desired characteristics by low-price priority.

2.2 3D modelling and finite element analysis

After applying the compiled information to the part under study, the second task is to design a 3D model able to be manufactured by the selected AM technique, and finally compare its properties with the original one. For the development of a 3D model of the piece, AutoCAD software was utilized. This computer-aided design software allows

Table 3 Sizing (grey shading in the table) and inflation configuration for couplings' mesh

Parameter	Value
Use adaptive sizing	Yes
Resolution	7
Mesh defeaturing	Yes
Transition	Slow
Span angle centre	Fine
Initial size seed	Assembly
Bounding box diagonal	0.19 m
Average surface area	$8.1 \cdot 10^{-4}$ m^2
Minimum edge length	$7.4 \cdot 10^{-5}$ m
Use automatic inflation	None
Inflation option	Smooth transition
Transition ratio	0.27
Maximum layers	8
Growth rate	1.2
Inflation algorithm	Pre
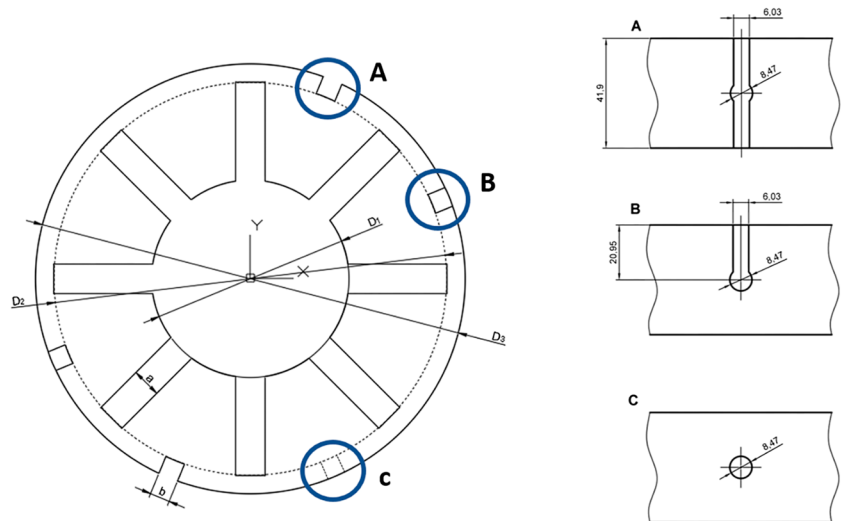
users to work in 2D drawing and 3D modelling, with mesh and solid surfaces. Once the spare part was 3D printed, to ensure that the prototype complies with the established performance requirements, the proceedings listed below have been followed: (i) requirements regarding the geometry are analysed from the component's data sheet and by measuring the dimensions of the original piece; (ii) material properties are extracted by testing; (iii) static simulations are carried out as a validation method and to try working conditions by finite element analysis (FEA); (iv) a real service working is used to test its final performance in the industry; (v) a topological optimization study for the redesigned coupling was carried out through nTopology software.

The 3D model was obtained by the AutoCAD software, and the AutoCAD geometrical design for each coupling was imported to ANSYS Workbench. The torsional stiffness was obtained from the manufacturer's data sheets summarized in Table 1.

For simulations, the coupling's body was considered as an annular one, and shear stress (τ) was calculated by Eq. 1 through the maximum torque (T_{max}), the section's external diameter (D_3) and the equivalent one (D_{eq}) to the inner empty area diameter (A_e), the last given by Eq. 2 (see Fig. 2 to clarify the used parameters).

$$\tau = \frac{T_{max} \cdot \frac{D_3}{2}}{\frac{\pi}{32} \cdot \left(D_3^4 - D_{eq}^4 \right)} \tag{1}$$

$$A_e = 8 \cdot \frac{D_2 - D_1}{2} \cdot a + \frac{\pi}{4} \cdot D_1^2 = \frac{\pi}{4} \cdot D_{eq}^2 \tag{2}$$

The minimum required safety rate is obtained by the product of three parameters (F1, F2, F3) given by the worst working conditions of a manhole pump able to triturate and transport medium masses in irregular operation, where the studied coupling is settled [23] (Table 2).

This CAD software allows working in 2D drawing and 3D modelling, combining meshes and solid surfaces with sizing and inflation parameters (Table 3). Sizing parameters define the size and the number of elements that make up the mesh, as well as the transition type between them. Inflation parameters, on the other hand, improve the resolution in those areas where greater efforts could be concentrated [24]. In the couplings studied, efforts were concentrated in the external incisions of the part. Figure 1c shows the meshing details.

The 3D models were printed using a RISE3D desktop printer. They were printed with a 0.4 mm nozzle at 210 °C, a printing temperature of 50 °C and a printing speed of 25 mm/s. In order to adapt the design of the coupling to 3D printing, the following actions were carried out: (i) design of support structures for the housings with considerable saving in time and material; (ii) modify the part filling to control the hardness using gyroid-type filling structures. Two infill parameters (60% and 80%) were selected, and wall thickness was 2 mm. The material used was the FilaFlex™ of 1.75 mm diameter.

After printing the redesigned couplings, mechanical properties were compared to the original ones. The Universal Test Machine SHIMADZU AGS-50kNXD was used to

Table 4 Dimensions in mm of original and 3D printed couplings

Measurements	Original	80% infill	60% infill
D_1	50.13	50.43	50.72
D_2	116.00	115.32	115.63
a	8.83	8.92	8.82
b	6.03	6.05	6.08
Height	41.90	39.80	39.90

Table 5 Shore A hardness measurements on the bottom and upper faces

Coupling	Face	Value
Original	Bottom	93.83 ± 0.62
	Upper	95.33 ± 0.47
80% infill	Bottom	75.17 ± 0.62
	Upper	87.17 ± 0.24
60% infill	Bottom	74.67 ± 0.70
	Upper	83.33 ± 0.94

Table 6 Maximum displacement, estimated and experimental Young's modulus

Coupling	Maximum displacement	Young's modulus estimated from manufacturer's data	Experimental Young's modulus
Original	1.45 mm	105 MPa	77.67 MPa
80% infill	4.60 mm	20 MPa	16.28 MPa
60% infill	7.07 mm	20 MPa	12.11 MPa

assess a simple and cyclical compression test. The simple compression test was carried out considering the maximum load values supported by the tested materials (15 kN for TPU). Moreover, an average compression velocity of 5 mm/min was used to achieve the force established [25]. A cyclic loading with 25 kN was applied in the z-direction of the structure to test its performance (Fig. 2). The Shore A hardness was tested in both faces with the Hildebrand HD3000 Durometer at 26 °C and with 34% of relative humidity.

Likewise, an engineering software developed by ANSYS was used to analyse static simulations by finite element, thus testing the new design under the original coupling working conditions. Finally, an actual service working was used to test their performance in the industry.

2.3 Eco-audit

An eco-audit, through GRANTA Edupack software [26], allowed to know and compare the energy consumption and the carbon footprint of the life cycle of each component, original and additive manufactured ones. This tool is one of the most suitable software of lifecycle impact assessment for sustainable design, being widely used in several researches [27–30]. For determining energy consumption, the software combines user-defined inputs with data drawn from databases of embodied energy of materials, processing energies and transport type [31]. To obtain a CO_2 footprint, the software uses conversion factors provided for the above-mentioned sources.

2.4 Generative design study

To optimise the manufacture through 3D printing, a generative design study of the spare part was carried out using the nTopology™ software (New York, USA). This is a new generation design tool oriented to additive manufacture parts as it works with really complex structures that can only be produced with AM technologies. This novel CAD/CAM engineering software is based on implicit modelling, where shapes are represented using implicit equations, and not with the traditional boundary representations (B-Reps) or complex surfaces non-uniform rational B-spline (Nurbs). This technology allows to align at the same level the scalar field values obtained from the simulation with FEA of the compression loads, with the three-dimensional modelling of the parts, permitting to adapt the width of the internal structure to the stress of the part defined in the simulation.

3 Results and discussion

3.1 Materials and method selection

The following requirements were crucial to obtain a flexible coupling: high tensile and torsional strength, shear resistance, flexibility, resistant to chemical substances and external agents such as humidity, and capacity of working between −40 and 80 °C. Furthermore, the material should be suitable for 3D printing. Accordingly, two materials were selected from the list presented by Bourell et al. [22], TPU
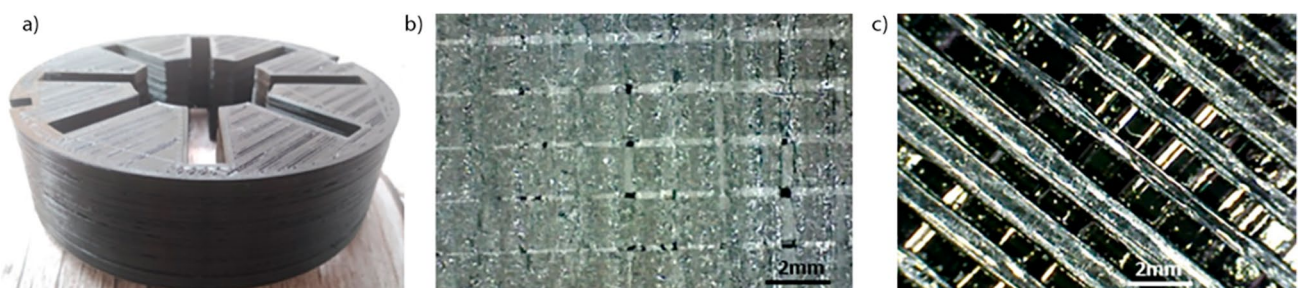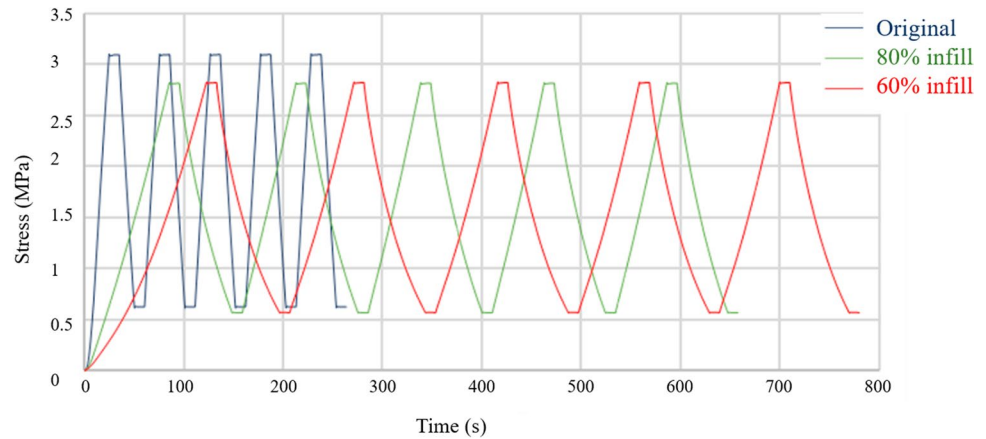

Fig. 3 **a** 3D printed coupling with 60% infill density. **b** Detail of the bottom face. **c** Detail of the upper face

Fig. 4 Time-evolution cyclical compression test at 25 k N in the original coupling (blue line), in the coupling with 80% infill (green line), and in the coupling with 60% infill (red line)

and polyamide (PA). The FFF and the multi jet fusion (MJF) developed by the HP enterprise were chosen as the most suitable AM methods. FFF allows working with elastomeric materials and desktop printers are indeed cheaper than other industrial printers. The MJF method allows rigid and flexible material to be used, thus obtaining pieces with isotropic mechanical properties. However, the main drawback is its medium-high cost that makes it economically inviable. However, MJF offers great mechanical and thermal properties in the final pieces, as well as great geometric precision [32, 33].

An FFF desktop printer and TPU were therefore selected considering their price and mechanical properties. Afterwards, the amount of both printing material and air inside the component was determined. These parameters were given by the infill percentage and pattern. Process parameters such as raster angle, layer thickness, infill percentage and printing speed influence the mechanical behaviour of printed parts [34]. Likewise, infill density should be between 60 and 100% to support considerable efforts.

3.2 Experimental comparative study

Figure 2 and Table 4 show the main dimension measurements taken from the FFF 3D printed prototypes using TPU with 60% and 80% infill. According to the information provided by the manufacturer, the mounting dimension in assembly should be 2.5 mm, with +0.7, 0.5 and 0.3 mm being the maximum tolerance axial, radial and angular, respectively. Furthermore, the values of the printed models were at permissible levels for their proper functioning.

The results of the Shore A hardness test are shown in Table 5. Shore A hardness was greater and similar in the two faces of the original coupling compared to the 3D printed ones. As for printed parts, the value of the Shore A hardness increased as infill density decreased due to greater air content. Furthermore, the difference between upper and bottom faces in the 3D printed couplings decreased from 13.8 to 10.4% when the filling percentage was decreased by 33%. The FFF method is based on the use of filament and tends to have rough finishes, where the filaments are defined depending on the size of the nozzle used for extrusion. These
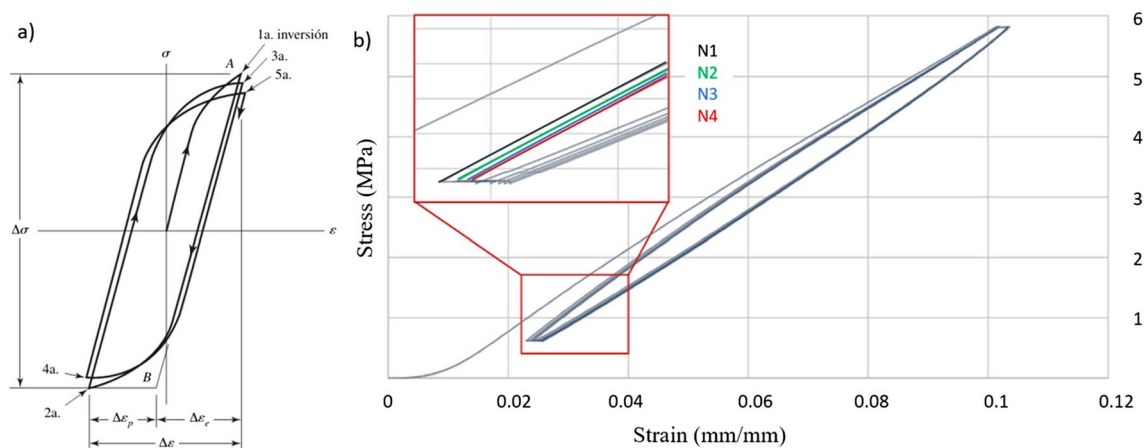
Fig. 5 a Stress-strain hysteresis loops. **b** Cyclic uniaxial compression test of the original coupling. The enlarged detail of the hysteresis cycle is highlighted in red. *N* indicates the cycle number
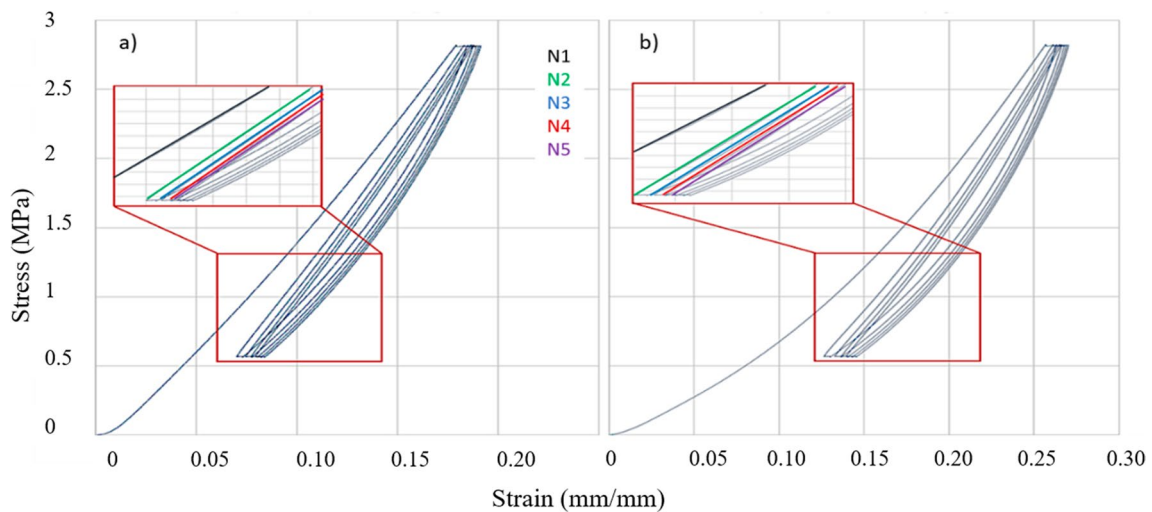
Fig. 6 a Stress-strain hysteresis loops of the coupling with 80% infill. **b** Stress-strain hysteresis loops of the coupling with 60% infill. The enlarged detail of the hysteresis cycle is highlighted in red in both graphics. *N* indicates the cycle number

surface irregularities, as well as the formation of rust in metallic components, could prematurely deteriorate the part as they could affect its correct lubrication, so the surface of the 3D printed parts should be studied.

Figure 3 shows a 3D printed coupling (a) in which both faces had various surface finishes: the surface used as bottom during manufacture showed a practically complete filling (b), while the upper face allowed the filament bead to be seen through slits; the filament bead had great levels of roughness (c). In addition, the direction of the filament can be seen on the entire lateral surface, tracing circular layers around the perimeter of the part. The function of the elastic coupling consisted in acting as a link between two metallic shafts, so the presence of coarse roughness would increase their friction and prevent them from slipping. Therefore, this increase in surface roughness should not be an inconvenience.

A simple uniaxial compression test was performed to the three parts, with a maximum load of 15 kN and an average compression velocity of 5 mm/min [25]. Table 6 shows the results of both the maximum displacement and the Young's modulus obtained by the test, as well as the estimated Young's modulus from manufacturer's data.

There were differences between the obtained and expected values. The original part had been used in industry and had been studied, so its mechanical properties had decreased because of the fatigue processes suffered by this type of element, thus justifying a decrease of 26% in the value of its Young's modulus. The two parts obtained by AM were not solid, so the modulus value established by manufacturers for solid materials (i.e., 20MPa) was not obtained. In fact, the variation of the actual modulus between the two 3D printed parts implied that one had been manufactured

with greater infill density. This statement was based on the Law of Mixtures proposed by Voigt in 1889 and considered the simplest homogenisation technique that can be applied to a composite material [35].

Figure 4 shows the behaviour upon cyclic loading. Although cycles looked quite similar, there were differences, specifically a greater displacement and an increase in the cycle time in the coupling with lower density values. Furthermore, the hold zone, where stress remains constant, seems to decrease for 80% and, especially for 60% infill parts, however, this phenomenon is just a visual effect of the graph, since the time required to recover the deformation increases significantly when density decreases. The effect of density on the compressive behaviour was reported by Fei Shen et al. [36], who studied the energy absorption capacity of spherical-shell lattice structures of TPU under cyclic compression loading, observing a cubic-like relationship between the compression force and energy absorption, as well as a decrease in energy absorption per unit volume when porosity increased. Before applying the cycles, the original and the 80% infill curves seemed to have a constant slope; however, the 60% infill curve had two slopes. This phenomenon has been previously seen in the ABS/TPU

Table 7 Yield strength and Tresca safety factor obtained by simulation

Coupling	Yield strength	Tresca safety factor
Original	40.00 MPa	14.46
80% infill	32.56 MPa	11.77
60% infill	24.22 MPa	8.76

Fig. 7 Deformation in mm of the simulated original coupling at a 15 kN compression test
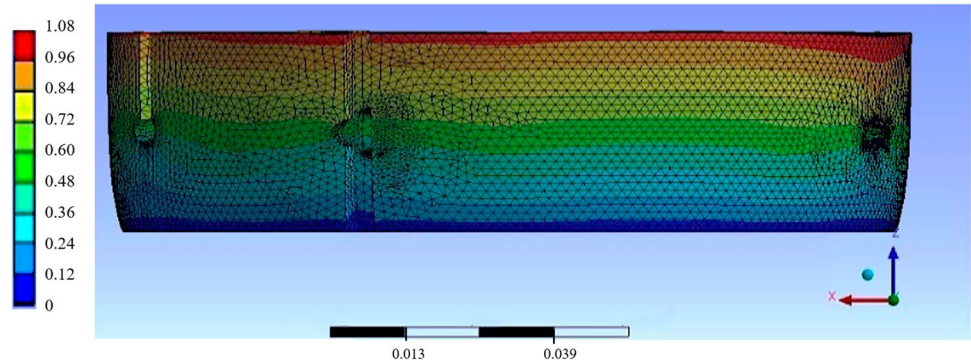
nanocomposite blend [37] and in the porous TPU obtained by 3D printing [38].

Once the material recovers the pre-stimulus situation, the properties may differ from the original ones. Energy dissipation implies that the loading stress is always higher than the unloading stress, a phenomenon known as the Mullins effect [39]. The stress-strain hysteresis loops shown in Fig. 5a correspond to a generic hysteresis cycle where the slope of the line AB represents the elastic modulus [40]. This graph shows the range of stresses ($\Delta\sigma$), the range of plastic strains ($\Delta\varepsilon p$) and the range of elastic strains ($\Delta\varepsilon e$), with the total strain ($\Delta\varepsilon$) being the sum of both ranges. Figure 5b shows the first five stress reversals of the original coupling. As can be seen in the hysteresis cycle inset highlighted in red, the material underwent softening behaviour during cyclic loading, with most of the softening being generated in the first cycle, due to the maximum displacement occurring between the first (N1) and the second cycle (N2). Stabilisation was observed after applying four cycles. The same phenomenon took place in the couplings obtained by AM (Fig. 6). Analogous behaviour has been observed by other researchers in pure TPU and 3D printed TPU honeycombs under in-plane compression stress [41]. A cyclic loading of elastomers produces an unrecoverable hysteresis energy loss depending on the molecular nature of the elastomer [39]. According to researchers, the stress-strain behaviour of TPUs is characterised by highly non-linear rate-dependent hyperelastic-viscoplasticity, where substantial energy dissipation is accompanied by shape recovery and softening [42].

3.3 In-service performance simulation

The studied part transmitted power to the inner-toothed area from one axis to another through the incisions in the part's external wall. The maximum shear stress value (τ_{max}) due to the torsional force varied depending on the distance between the studied area and the torque origin.

A value of 1.38 MPa shear stress (τ) was generated when applying the maximum torque (T_{max}). In simulations, the coupling body was considered as an annular body. Motor characteristics were unknown, so a Manhole Pump was considered to triturate and transport medium masses in irregular operation under the worst in-service performance. As a result, the minimum safety factor amounted to 4.55, hence couplings will work appropriate at the machine (Table 7).

Figure 7 shows the deformation of the simulated original coupling under a 15 kN compression test in a coloured scale. The maximum displacement value should be in the upper area of the model and decrease to the lower zone.

Table 8 includes the maximum simulated and measured displacement obtained in 3D printed couplings. As for the coupling with 80% infill, the calculated properties were close to reality. However, the displacement in the original and in the simulated ones with 60% infill were slightly lower than those expected. Nevertheless, the deviation of 27.42% represented a difference of 0.40 mm, so the properties calculated by testing and simulating were valid and useful for torsion simulation.

Figure 8 shows the distribution of shear stress because of the twisting moment applied to the coupling. As expected, the maximum tangential effort (τ) of 1.72 MPa was obtained in the lateral perimeter of the pieces. Likewise, the maximum simulated value of 1.72 MPa was slightly greater than the 1.38 MPa tangential effort obtained through the maximum torque. This tangential effort, as shown in the Eqs. 1 and 2, depended on the part's geometry, not on its properties, so the same value was

Table 8 Simulated and experimental maximum displacement values and its deviation

Coupling	Simulated	Measured	Error
Original	1.08 mm	1.49 mm	27%
80% infill	4.76 mm	4.60 mm	3%
60% infill	6.38 mm	7.17 mm	11%

Fig. 8 Shear stress (MPa) in a coloured scale after applying a 500 Nm torque in the couplings. Detail of the stress generated in critical areas
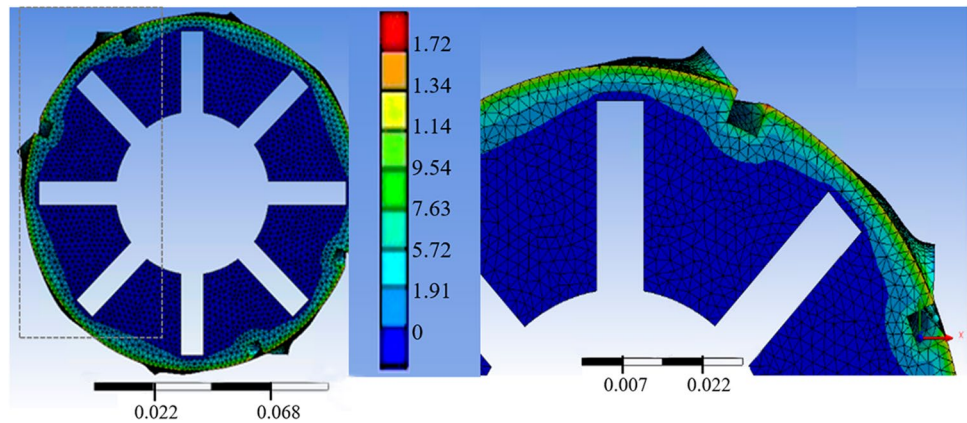
determined for each coupling. However, the deflection suffer from the part depends on material properties, given different values for each coupling.

Safety factors were re-calculated, resulting in 11.65, 9.48 and 7.06 in original, 80% and 60% infill, respectively. Accordingly, the values still met the minimum requirements for an appropriate operation behaviour.

3.4 Eco-Audit study

Likewise, economic factors should be considered, but there are other parameters, such as environmental ones, which could significantly influence values. Information about the origin of the material, the manufactured process, the end-of-life (EoL), the conveyance, the distance from the manufactured to the industry and the use of couplings during their life cycle required to carry out an eco-audit are gathered in Table 9.

Table 10 shows the values of energy consumption (in MJ) and carbon footprint (CO_2 in kg) for each coupling. The use stage represents both the highest energy consumption and CO_2 emissions. According to the European CO_2 Trading

System, the tax is about 83€ per ton of CO_2 emitted, so replacing the original coupling would imply economic savings of €1332 and €2740 by using couplings with 80% and 60% infill, respectively.

3.5 Generative design study

From the results of ANSYS simulations, a CSV (Comma Separated Values) file with the information related to the scalar field of the compressive stresses to which the coupling was subjected during its in-service performance was obtained (Fig. 9a). This information was imported to the nTopolgy software, and the stress field was presented and aligned to the part model, showing the specific stress levels of the part at each point of its spatial geometry (Fig. 9b). Stablishing as primary study a range from 0.1 to 10 mm infill thickness for the lower and upper limits of the stress demands and a constant shell value of 3 mm, this novel approach used them to define a ramp of thickness values that coincided with the mechanical demands at each point, optimising its performance and reducing weight up to 0.32 kg as an alternative design process (Fig. 9c).

Table 9 Eco-audit tool inputs

Coupling	Original	80% infill	60% infill
Material	TPU	TPU	TPU
Mass	0.38kg	0.31kg	0.28kg
Primary process	Polymer moulding	Polymer extrusion	Polymer extrusion
Conveyance	Light goods vehicle	Light goods vehicle	Light goods vehicle
Distance from manufacturer	1100 km	100 km	100 km
EOL	2.8 years	2.7 years	2.6 years
Country	Spain	Spain	Spain
Incoming and outgoing energy	Fossil fuels to mechanic	Fossil fuels to mechanic	Fossil fuels to mechanic
Power	22 kW	22 kW	22 kW
Use	365 days/year	365 days/year	365 days/year
Use	24 hours/year	24 hours/year	24 hours/year

Table 10 Eco-audit reports

Coupling	Original		80% infill		60% infill	
Stage	Energy (MJ)	Carbon footprint (kg CO_2)	Energy (MJ)	Carbon footprint (kg CO_2)	Energy (MJ)	Carbon footprint (kg CO_2)
Material	31.20	1.220	25.4	0.994	23.0	0.898
Manufacturing	7.150	0.536	1.89	0.142	1.710	0.128
Transport	0.920	0.066	0.07	0.005	0.062	0.004
Use	$6.48 \cdot 10^6$	$4.66 \cdot 10^5$	$6.24 \cdot 10^6$	$4.50 \cdot 10^5$	$6.01 \cdot 10^6$	$4.33 \cdot 10^5$
EOL	0.076	0.005	0.217	0.015	0.196	0.014
EOL recovered energy	0	0	−16.8	−0.656	−15.2	−0.593

This weight is slightly higher than the 80% infill model presented above.

4 Conclusion

This study explores the implementation of 3D printing technologies in the chemical industry, through the redesign of spare parts, particularly a flexible coupling. The TPU coupling printed by FFF has been technically feasible from a mechanical and environmental perspective.

Although the Shore A hardness of the 3D printed couplings was 6.26% lower than the original one, the couplings redesigned using 3D printing met the safety factors indicated by manufacturers. Nevertheless, fatigue resistance was expected to be lower in AM components because of the hysteresis cycles observed in each coupling in the cycling compressive test.

When the couplings were subjected to a compressive stress of 2 MPa, the maximum displacement increased 3 times (80% infill) and 4 times (60% infill) compared to the original one, with no permanent deformation.

Though coupling 3D printed with gyroid with 80% infill showed the best compromise of strength-weight, the part redesigned with 60% infill required less printing time (6 h less) and material (30% less), so it was more appropriate to be used.

While energy consumption and carbon dioxide emissions in use stage were similar in the original and redesigned ones, 74% (80% infill) and 76% (60% infill) of energy was saved in the manufacturing stage. The same percentage was obtained in CO_2 emission reductions. Additive manufacturing components reduced CO_2 emissions by 4% (in the coupling with 60% infill) and 7% (in the coupling with 80% infill) in their total life cycle, thus representing an economic saving of €2740 and €1332, respectively, per coupling due to CO_2 emission fees.
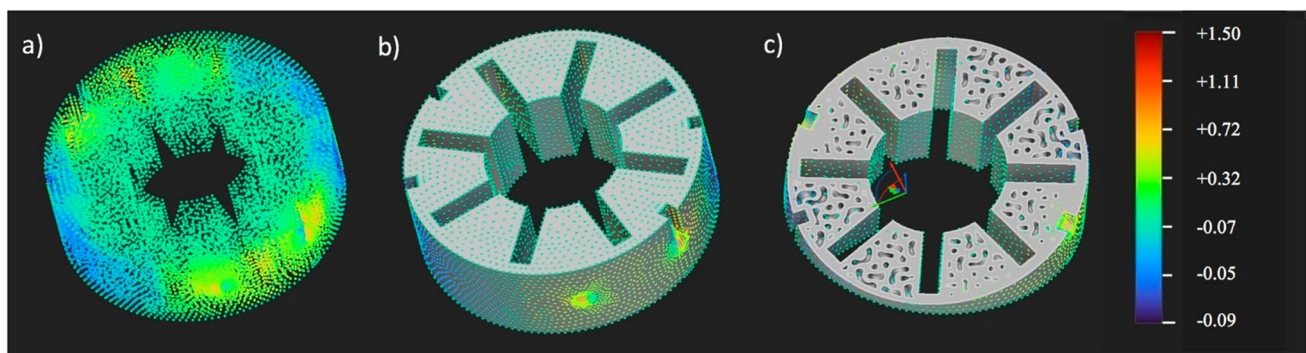

Fig. 9 **a** Stress scalar field (MPa) obtained from FEA. **b** Scalar field aligned with the part. **c** Optimized infill density of the part

The field-driven design study allows couplings' material to be concentrated in critical areas to increase hardness and reduce deformations, resulting in a weight reduction of up to 15.8% without modifying coupling's density. Further studies could consider a simulation driven design approach with generative design for redesigned coupling at a higher level of detail to enhance the operation behaviour of the component.

Declarations

References

1. Boyer KK, Ward PT, Leong GK (1996) Approaches to the factory of the future. An empirical taxonomy. J Oper Manag 14(4):297–313. https://doi.org/10.1016/S0272-6963(96)00093-9
2. Rüßmann M, Lorenz M, Gerbert P, Waldner M (2015) Industry 4.0: The Future of Productivity and Growth in Manufacturing Industries. Bost Consult Gr 9(1):54–89
3. Sirichakwal I, Conner B (2016) "Implications of Additive Manufacturing for Spare Parts Inventory", 3D Print. Addit Manuf 3(1):56–63. https://doi.org/10.1089/3dp.2015.0035
4. Westerweel B, Basten RJI, van Houtum GJ (2018) Traditional or Additive Manufacturing? Assessing Component Design Options through Lifecycle Cost Analysis. Eur J Oper Res 270(2):570–585. https://doi.org/10.1016/j.ejor.2018.04.015
5. Holmström J, Partanen J, Tuomi J, Walter M (2010) Rapid manufacturing in the spare parts supply chain: Alternative approaches to capacity deployment. J Manuf Technol Manag 21(6):687–697. https://doi.org/10.1108/17410381011063996
6. Liu P, Huang SH, Mokasdar A, Zhou H, Hou L (2014) The impact of additive manufacturing in the aircraft spare parts supply chain: supply chain operation reference (scor) model based analysis. Prod Plan Control 25(13–14):1169–1181. https://doi.org/10.1080/09537287.2013.808835
7. Kostidi E, Nikitakos N, Progoulakis I (2021) Additive manufacturing and maritime spare parts: Benefits and obstacles for the end-users. J Mar Sci Eng 9(8):895. https://doi.org/10.3390/jmse9080895
8. Westerweel B, Basten R, den Boer J, van Houtum GJ (2021) Printing Spare Parts at Remote Locations: Fulfilling the Promise of Additive Manufacturing. Prod Oper Manag 30(6):1615–1632. https://doi.org/10.1111/poms.13298
9. Delic M, Eyers DR (2020) The effect of additive manufacturing adoption on supply chain flexibility and performance: An empirical analysis from the automotive industry. Int J Prod Econ 228:107689. https://doi.org/10.1016/j.ijpe.2020.107689
10. Abella RJ, Daschbach JM, McNichols RJ (1994) Reverse engineering industrial applications. Comput Ind Eng 26(2):381–385. https://doi.org/10.1016/0360-8352(94)90071-X
11. Jeong DE et al (2021) Assemblies of putative SARS-CoV2-spike-encoding mRNA sequences for vaccines BNT-162b2 and mRNA-1273. GitHub, no. i, pp 0–3. Available online: https://virological.org/t/assemblies-of-putative-sars-cov2-spike-encoding-mrna-sequences-for-vaccines-bnt-162b2-andmrna-1273/663
12. Froes FH, Boyer R (eds) (2019) Additive manufacturing for the aerospace industry. Elsevier
13. Attaran M (2017) The rise of 3-D printing: The advantages of additive manufacturing over traditional manufacturing. Bus Horiz 60(5):677–688. https://doi.org/10.1016/j.bushor.2017.05.011
14. Campbell TW (2012) Technologies, Potential, and Implications of Additive Manufacturing, *Cbpp.Uaa.Alaska.Edu*, [Online]. Available: http://www.cbpp.uaa.alaska.edu/afef/Additive%20MFG%20.pdf. Accessed 10 Nov 2022
15. Bourell D et al (2017) Materials for additive manufacturing. CIRP Ann Manuf Technol 66(2):659–681. https://doi.org/10.1016/j.cirp.2017.05.009
16. Ngo TD, Kashani A, Imbalzano G, Nguyen KTQ, Hui D (2018) Additive manufacturing (3D printing): A review of materials, methods, applications and challenges. Compos Part B Eng 143:172–196. https://doi.org/10.1016/j.compositesb.2018.02.012
17. "EU Emissions Trading System." https://www.epa.ie/our-services/licensing/climate-change/eu-emissions-trading-system-/. Accessed 27 Sept 2022
18. Federe N (2020) Topology optimization of automotive sheet metal part using altair inspire. International Journal of Engineering and Management Sciences 5(3):143–150. https://doi.org/10.21791/IJEMS.2020.3.15.focus
19. Tyflopoulos E, Steinert M (2022) A comparative study of the application of different commercial software for topology optimization. Appl Sci 12(2):611
20. Ntopology (2021) "Field-Driven Design", George Allen; nTopology Next-generation Des Eng Softw [Online]. https://www.ntop.com/field-driven-design/. Accessed 10 May 2023
21. Becergen B, Cakmak M, Maral MF, Dayanc A, Karakoc F (2022) Design Approaches on Inner Bodies of Gears with Methods Topology Optimization and Lattice Structures Topoloji Optimizasyonu ve Kafes Yapıları Yöntemleriyle Dişlilerin İç Gövdelerinde Tasarım Yaklaşımları. 39:85–90. https://doi.org/10.31590/ejosat.1144818
22. Bourell D et al (2017) Materials for additive manufacturing. CIRP Ann 66(2):659–681

23. Samiflex (2020) Catálogo de acoplamientos elásticos. Available online: http://www.citsa.com/dwn/PDFes/2020/Samiflex_Esp.pdf. Accessed 9 Oct 2021
24. ANSYS. https://www.ansys.com/. Accessed 06 Mar 2023
25. Jerabek M, Major Z, Lang RW (2010) Uniaxial compression testing of polymeric materials. Polym Test 29(3):302–309
26. Ashby M, Brechbühl E, Vakhitova T, Vallejo A (2021) Social Life-Cycle Assessment and Social Impact Audit Tool: A white paper, *ANSYS Granta Des.*, no June, pp 1–21, 2019, [Online]. Available: https://grantadesign.com/teachingresources/papslcen19/. Accessed 07 Mar 2023
27. Koronis G, Silva A (2018) Green composites reinforced with plant-based fabrics: Cost and eco-impact assessment. J Compos Sci 2(1):9–15. https://doi.org/10.3390/jcs2010008
28. Nijssen JPA, Faludi J, van Ostayen RAJ (2021) An eco-impact design metric for water lubricated bearings based on anticipatory Life Cycle Assessment. J Clean Prod 321:128874. https://doi.org/10.1016/j.jclepro.2021.128874
29. Grinberg D et al (2021) Eco-audit of conventional heart surgery procedures. Eur J Cardio-thoracic Surg 60(6):1325–1331. https://doi.org/10.1093/ejcts/ezab320
30. Gradin KT, Åström AH (2018) Evaluation of an Eco Audit tool - through an LCA of a novel car disc brake. DS 91: Proceedings of NordDesign 2018, Linköping, Sweden, 14th–17th August 2018
31. "Ansys Granta EduPack Help." https://support.grantadesign.com/resources/grantaedupack/2022R2/en/help/index.htm#t=html/eco/eco_audit_about.htm. Accessed 07 Mar 2023
32. Ziaee M, Crane NB (2019) Binder jetting: A review of process, materials, and methods. Addit Manuf 28(June):781–801. https://doi.org/10.1016/j.addma.2019.05.031
33. Fradl D, Panditaratne J, Bi J, Fu R, Oancea V (2017) Finite Element Simulation of the Multi Jet Fusion (MJF^TM) Process using Abaqus Dan Fradl, Jay Panditaratne. Sci Age Exp no. October, pp 440–469, [Online]. Available: https://pdfs.semanticscholar.org/fb66/17aab5ff74f47709ebfecb694d32f23ceff2.pdf. Accessed 10 Oct 2021
34. Algarni M, Ghazali S (2021) Comparative Study of the Sensitivity of PLA, ABS, PEEK, and PETG's Mechanical Properties to FDM Printing Process Parameters. Curr Comput-Aided Drug Des 11(8):995. https://doi.org/10.3390/cryst11080995
35. Voigt W (1889) On the relation between the elasticity constants of isotropic bodies. Ann Phys Chem 274:573–587
36. Shen F et al (2016) Energy absorption of thermoplastic polyurethane lattice structures via 3d printing: modeling and prediction. Int J Appl Mech 8(7). https://doi.org/10.1142/S1758825116400068
37. Tecnol C (2010) Análisis del Módulo Elástico y Resistencia a la Ruptura en Mezclas de Nanocompuestos de ABS/TPU. Concienc Tecnológica 39:5–11
38. Lee H, Eom RI, Lee Y (2019) Evaluation of the mechanical properties of porous thermoplastic polyurethane obtained by 3D printing for protective gear. Adv Mater Sci Eng. https://doi.org/10.1155/2019/5838361
39. Lee K, Lee B, Kim C, Kim H, Kim K, Nah C (2005) Stress-strain behavior of the electrospun thermoplastic polyurethane elastomer fiber mats. Macromol Res 13(5):441–445. https://doi.org/10.1007/BF03218478
40. Budynas RG, Nisbett JK (2008) Shigley's mechanical engineering design, 8th edn. McGraw-Hill, New York
41. Qi MC, Boyce HJ (2005) Stress–strain behavior of thermoplastic polyurethanes. Mech Mater 37(8):817–839
42. Cho H et al (2017) Deformation mechanisms of thermoplastic elastomers: Stress-strain behavior and constitutive modeling. Polymer (Guildf) 128:87–99. https://doi.org/10.1016/j.polymer.2017.08.065

Publisher's note Springer Nature remains neutral with regard to jurisdictional claims in published maps and institutional affiliations.